Experiments on mixed convection in a vented differentially side-heated cavity filled with a coarse porous medium

Ataei-Dadavi, Iman; Chakkingal, Manu; Kenjeres, Sasa; Kleijn, Chris R.; Tummers, Mark J.

Citation (APA)
Ataei-Dadavi, I., Chakkingal, M., Kenjeres, S., Kleijn, C. R., & Tummers, M. J. (2020). Experiments on mixed convection in a vented differentially side-heated cavity filled with a coarse porous medium. *International Journal of Heat and Mass Transfer*, *149*, Article 119238. https://doi.org/10.1016/j.ijheatmasstransfer.2019.119238

Important note
To cite this publication, please use the final published version (if applicable).
Please check the document version above.

Experiments on mixed convection in a vented differentially side-heated cavity filled with a coarse porous medium

Iman Ataei-Dadavi [a],*, Manu Chakkingal [a], Sasa Kenjeres [a], Chris R. Kleijn [a], Mark J. Tummers [b]

[a] Department of Chemical Engineering, Delft University of Technology, Van der Maasweg 9, 2629HZ Delft, Netherlands
[b] Department of Process and Energy, Delft University of Technology, Leeghwaterstraat 39, 2628CB Delft, Netherlands

ARTICLE INFO

ABSTRACT

This paper reports on an experimental study of mixed convection flow and heat transfer in a vented, differentially side-heated cubical cavity filled with a porous medium consisting of relatively large solid low-conductivity spheres. Rayleigh numbers and Reynolds numbers are varied over the ranges $6 \times 10^6 < Ra < 7 \times 10^7$ and $240 < Re < 4250$, respectively, for a fixed Prandtl number of $Pr = 6.75$, thus covering more than three decades in Richardson numbers $Ri = Ra/(Re^2\ Pr)$. Heat transfer measurements were combined with measurements of the velocity field (using particle image velocimetry) and the temperature field (using liquid crystal thermography) to better understand the dependence of the Nusselt number, Nu, on the Richardson number. We observed three different flow and heat transfer regimes depending on the Richardson number. For $Ri < 10$, the flow structure and the Nusselt number scaling are similar to those for the pure forced convection, i.e., the Nusselt number scales as $Nu \sim Re^{0.61}$ independent of Rayleigh number. For $Ri > 40$, natural convection dominates the flow in the vicinity of the heating wall. The Nusselt number becomes less sensitive to the Reynolds number and is mainly determined by the Rayleigh number. In the intermediate regime for $10 < Ri < 40$, the upward directed natural convection flow at the heating wall competes with the downward directed forced flow leading to a minimum effective Nusselt number. A Nusselt number correlation is derived that is valid in the range $0.1 < Ri < 100$ covering all three regimes.

1. Introduction

Natural convection in closed cavities has been among the most widely studied topics in fluid dynamics due to its simple geometry and relevance to many engineering applications. Natural convection is characterized by the Rayleigh number, Ra, which measures the strength of the buoyancy forces relative to diffusive forces, and the Prandtl number, Pr, which is the ratio of the kinematic viscosity to the thermal diffusivity of the working fluid. When inlet and outlet vents are added to such a cavity, forced convection is introduced to the system as well, and, as a consequence, the Reynolds number, *Re*, also plays a role. Mixed convection is a result of the interaction between natural and forced convection and their relative strength is measured by the Richardson number $Ri = Ra/(Re^2 Pr)$. Mixed convection in vented cavities has attracted extensive attention during the past decades due to its application in, for exam-

ple, electronics cooling [1,2], indoor air conditioning [3–5], solar ponds [6], and energy storage systems [7]. Various vented mixed convection configurations with different heating/cooling sources and inlet/outlet locations have been studied and the results have been reported in the form of flow and temperature fields and dimensionless heat transfer coefficients (i.e., Nusselt numbers, Nu) for a range of Rayleigh and Reynolds numbers [2–4, 8–16]. These studies are almost exclusively numerical studies solving the Navier-Stokes equations for two-dimensional geometries. Singh and Sharif [9] conducted a numerical study of a vented cavity with differentially heated side walls. They examined six different configurations of inlet and outlet locations and determined Nusselt numbers and spatially-averaged temperatures for Reynolds numbers from 50 to 500 and Richardson numbers from 0 to 10. They concluded that the configurations in which forced and natural convection assist each other produce more effective cooling. Deng et al. [4] numerically studied airflow and heat/contaminant transport structures in a vented cavity with discrete heat and contamination sources. They observed different transport structures and ventilation modes de-

Nomenclature

c_p	Specific heat capacity, J/kg.K
d	Diameter of spheres, m
g	Gravitational acceleration, m/s^2
h	Height of the inlet/outlet ports, m
H	Inner height of the heating/cooling walls, m
k	Thermal conductivity, W/m.K
L	Inner dimension of the cavity, m
Nu	Nusselt number
Nu$_{eff}$	Effective Nusselt number
P	Electrical power supplied to the hot wall, W
Pr	Prandtl Number
Q_{loss}	Rate of heat loss, W
Q_{flow}	Rate of heat carried by the outflow, W
Q_{total}	Rate of heat supplied to the hot wall, W
Ra	Rayleigh Number
Re	Reynolds Number
Ri	Richardson Number
t	Time, s
T	Temperature, K
u_{in}	Bulk inflow/outflow velocity, $\dot{V}/(h \times L)$, m/s
v_z	Vertical velocity component, m/s
$\dot{V}$	Volumetric flowrate, m^3/s
x, y, z	Cartesian coordinates, m

Greek symbols

α	Thermal diffusivity, m^2/s
β	Thermal expansion coefficient, 1/K
ν	Kinematic viscosity, m^2/s
ρ	Density, kg/m^3

Subscripts

c	Cold
h	Hot
s	Solid
f	Fluid
in	Inflow
out	Outflow
FC	Pure forced convection
NC	Pure natural convection

pending on the relative strength of natural convection and forced convection, which is important in determining the indoor air environment. Papanicolaou and Jaluria [2] numerically studied mixed convection in a vented cavity with an isolated thermal source for Reynolds numbers between 50 and 2000 and Richardson numbers between 0 and 10. They found a general trend of increase of the average heat transfer rate from the source to the airflow when the Richardson number increases at a fixed Reynolds number as well as when the Reynolds number increases at a fixed Richardson number. They also reported on the effect of the location of the heat source and the outlet port.

Mixed convection in vented cavities filled with porous media or solid obstacles has several industrial applications, for example in grain storage, food storage, solar collectors, steel making furnaces, and electronics cooling. Despite its practical relevance, it has received much less attention than the case without porous media. Mahmud and Pop [17] were the first to publish on mixed convection in vented cavities filled with a porous medium. They numerically studied two-dimensional steady mixed convection using the Darcy flow model for porous medium Peclet numbers between 0.1 and 100, porous medium Rayleigh numbers between 0.1 and 1000, and inlet width to cavity height ratios between 0.1 and 0.6. The studied cavity was heated/cooled at the left wall and the forced flow was directed along the hot/cold wall with inlet and outlet vents at the top and bottom of the wall. They found that the flow pattern can change from a unicellular flow to a multicellular flow depending on the inlet width ratio, Peclet number, and Rayleigh number. Bhuiyan et al. [18] performed a similar study but considered three different cavity aspect ratios. Other researchers have studied vented cavities partially filled with porous media [19,20]. These studies used the Darcy model and its extensions, and solved volume-averaged continuum equations for the fluid and solid constituents.

In many of the above-mentioned applications of mixed convection in vented cavities, the porous medium consists of relatively large grains/obstacles. An example is the mixed convection at the hearth of steelmaking blast furnaces where the liquid iron is collected and tapped off [21]. The hearth is filled with relatively large coke particles with a typical size up to approximately 100 mm. With the hot liquid iron flowing in from the top, and leaving from the exit taphole, while the walls of the hearth are being cooled, the flow of liquid iron in the hearth is a mixed convection flow in a coarse-grained porous medium. Other examples include electronics cooling with relatively large electronic components [22] and cooling and storage of food packages and agricultural products [23]. In these cases, the pore length scale is not small compared to the flow and thermal length scales, and the validity of the Darcy model and the volume-averaged porous continuum approach is questionable. Moreover, for coarse porous media, it becomes more important to capture the details of the flow field and the temperature distribution at the pore-scale and to resolve the strong interaction between the flow and the solid grains. In this regard, a few of our recent studies have considered natural convection in closed cavities containing relatively large solid spheres at the pore level both experimentally [24,25] and numerically [26].

This study focuses on mixed convection in vented cavities filled with coarse-grained porous media. The objective is to provide detailed experimental data on the heat transfer scaling as a function of Reynolds and Rayleigh numbers. For this purpose, we used a cubical cavity with differentially heated side walls equipped with an inlet at the heating side and an outlet at the cooling side. The cavity is packed with relatively large solid spheres. To better understand the heat transfer results, we also determined the velocity fields and temperature fields in the pores by using optical measurement techniques in conjunction with a refractive index matched porous medium.

2. Experimental setup

The experimental setup consists of a cubical cavity with an inner dimension of $L = 77$ mm (see Fig. 1a). The cavity has one hot and one cold side wall which are made of copper and the other four walls are made of 4 mm thick glass. The hot wall was heated by an electrical foil heater (Minco HK5955) and the cold wall was internally cooled with water from a temperature-controlled water circulator (Julabo FP51-SL). To minimize the heat leakage, the glass walls and the heating wall were completely insulated during heat transfer measurements using thick polystyrene sheets (see Fig. 1a). The cavity is equipped with an inlet port at the heating wall and an outlet port at the cooling wall with each port having an internal size of $h \times L = 10$ mm $\times$ 77 mm. The remaining heating/cooling area is $H \times L = 62$ mm $\times$ 77 mm (see Fig. 1a). Fig. 1b illustrates two different mixed convection configurations A and B, and a pure forced convection configuration C considered in this study. The main focus of this study is on configuration A in which the inlet port is at the top of the heating wall and the outlet port at the bottom of the cooling wall. For comparison, a few experiments were performed in configuration B which results from rotating the same cavity positioned in configuration A about the
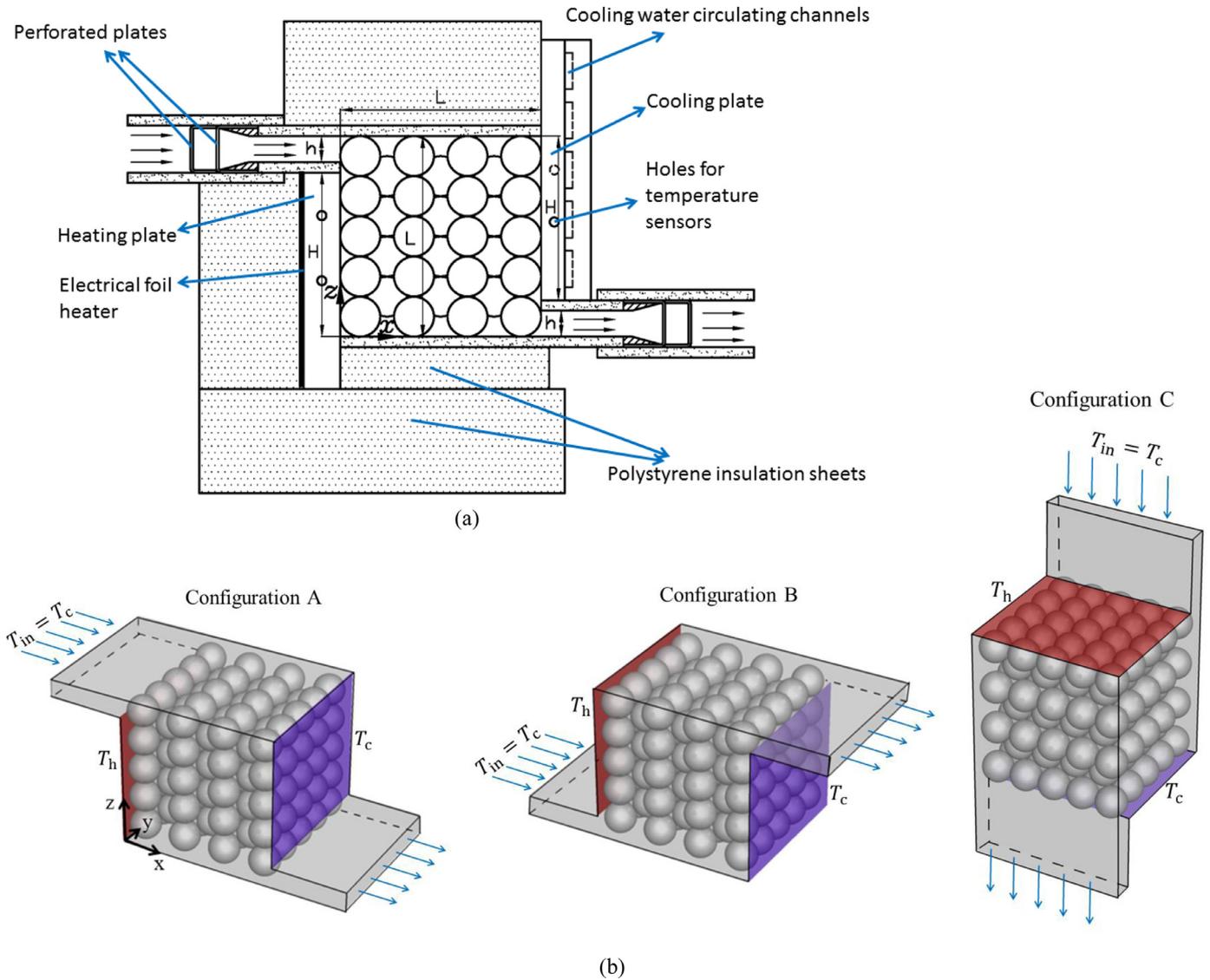
Fig. 1. The mixed convection cavity filled with d/L = 0.20 spheres in BCT packing: (a) Drawing and components of the cavity (configuration A), (b) Schematic view of the two studied mixed convection configurations A and B, and the pure forced convection configuration C. In all experiments the same cavity was used positioned in three different ways (Configuration A, B, and C). Results will be presented in the Cartesian coordinate system shown in Fig. 1b.

x-axis. In configuration B, the inlet port is located at the bottom of the heating wall and the outlet port at the top of the cooling wall. To obtain pure forced convection data points, the same cavity was rotated about the y-axis such that the heating wall is at the top and the cooling wall is at the bottom, see configuration C in Fig. 1b. In this configuration, there is no natural convection and only forced convection takes place. In the heat transfer experiments, the cavity was filled with polypropylene spheres with a diameter $d = 15.3$ mm ($d/L = 0.20$) and solid-to-fluid conductivity ratio of $k_s/k_f = 0.32$. The spheres were packed in a Body-Centered Tetragonal (BCT) packing structure (see Fig. 1).

The temperature of the heating and cooling walls, T_h and T_c, were monitored by four ultra-precise four-wire RTD sensors (Omega RTD-3–1PT100K2528-1M-T-1/10) with an inaccuracy of $\pm$ 0.03 °C. The same type of RTD sensors were used to measure the inflow temperature T_{in} and the outflow temperature T_{out}. The inflow and the cold wall were kept at the same temperature $T_{in} = =T_c$. The Rayleigh number is determined using the temperature difference between the heating wall and the inflow/cooling wall as in

$$Ra = \frac{\beta g (T_h - T_{in}) H^3}{\nu \alpha}, \tag{1}$$

where g is the gravitational acceleration and β, ν and α are the thermal expansion coefficient, the kinematic viscosity, and the thermal diffusivity of the working fluid, respectively. The Nusselt number is determined using the electrical power supplied to the heating wall P as in

$$Nu = \frac{P - Q_{loss}}{kH(T_h - T_{in})}, \tag{2}$$

where k is the thermal conductivity of the working fluid. Water was used as the working fluid in all the experiments. Q_{loss} is the minor heat loss and is determined by measuring the heat transfer in the water-filled vented cavity positioned as in configuration C (see Fig. 1b), with closed inflow and outflow. In this situation, both natural and forced convection are inactive and the fluid is stagnant so that only conduction occurs. The measured heat transfer minus the known conductive heat transfer through the stagnant water layer only is considered as the heat loss in this system. The water inflow into the cavity was supplied by a temperature-controlled water bath (Julabo F32-HE). A rotary vane pump (Fluid-o-Tech PA111) was used to provide a constant volumetric flowrate from the water bath into the cavity. A variable frequency drive (Hitachi L100) was used to vary the volumetric flowrate by regulating

the rotational speed of the pump motor. The volumetric flowrate was measured and monitored using a magnetic flowmeter (MAG-VIEW MVM-002-Q). The Reynolds number is determined using the inflow volumetric flowrate $\dot{V}$ as in

$$Re = \frac{u_{in}L}{\nu} = \frac{\dot{V}}{\nu h}, \qquad (3)$$

where $u_{in} = \dot{V} / (h \times L)$ is the bulk velocity of the water inflow/outflow. Using the Rayleigh and Reynolds numbers, the Richardson number can be obtained from

$$Ri = \frac{Ra}{PrRe^2}, \qquad (4)$$

where Pr is the Prandtl number of the working fluid. For water, at room temperature (22 °C) the Prandtl number is 6.75. In Section 3.5. we study how the heat generated at the heating wall is distributed between the two heat removal pathways: the cooling wall, and the outflow. For this purpose, we introduce another dimensionless number which is the ratio of the heat leaving the cavity by the outflow, Q_{flow}, and the total heat supplied to the hot wall, Q_{total}, as in

$$\frac{Q_{flow}}{Q_{total}} = \frac{\rho \dot{V} c_p (T_{out} - T_{in})}{P}, \qquad (5)$$

where ρ and c_p are the density and the specific heat capacity of the working fluid.

In this study, the Rayleigh number is varied over the range $6 \times 10^6 < Ra < 7 \times 10^7$ by varying the temperature difference $T_h - T_{in}$ between approximately 2 °C and 20 °C. The Reynolds number is varied over the range $240 < Re < 4250$ by varying the incoming volumetric flowrate from 2.4×10^{-6} m³/s to 4.2×10^{-5} m³/s. Consequently, the Richardson number is varied over a wide range of three decades, i.e., $0.1 < Ri < 100$. Depending on the set temperature difference $T_h - T_{in}$ and the set flowrate $\dot{V}$, the uncertainties in the measured Reynolds, Rayleigh, and Nusselt numbers are between 1.7% and 3.6%, 1.8% and 3.9%, and 1.5% and 3.7%, respectively. The resulting uncertainty for the Richardson number is between 3.9% and 8.2%.

As discussed in [24], refractive index matching of water and hydrogel spheres enables the use of optical measurement techniques for thermally-driven flows in porous media. In this study, we used hydrogel spheres in water ($k_s/k_f = 1$) to make a refractive index matched porous medium to be able to perform Particle Image Velocimetry (PIV) and Liquid Crystal Thermography (LCT) measurements. Hydrogel spheres with a diameter of approximately 15.3 mm ($d/L = 0.20$) were packed in a BCT structure. The PIV and LCT images were taken at the vertical plane $y/L = 0.4$, see Fig. 1.

Details of the PIV experimental setup are reported in [24]. The post-processing of PIV images was conducted using the commercial software Davis 8.4.0. A three-pass cross-correlation with final interrogation area of 16×16 pixels and 50% overlap was used to obtain velocity fields with a vector resolution of 0.60 mm. The time difference between the PIV image pairs, Δt, was varied from $\Delta t = 3$ ms at the highest flowrate to $\Delta t = 30$ ms at the lowest flowrate in order to have a maximum particle displacement of around 8 pixels. The mean velocity fields were obtained by averaging over 7200 instantaneous velocity fields that were acquired at 2 Hz. It was checked that, during the 1 h duration of measuring the mean velocity fields, the hot and the cold wall temperatures varied by less than 1% of the lowest temperature difference and the liquid flowrate varied by less than 3% of the lowest flowrate.

The LCT measurements were performed to determine the temperature distribution at the pore level in the porous medium. The LCT experimental setup is described in detail in [24]. The useful temperature range of the thermochromic liquid crystals used in this study (Hallcrest R25C60W) was determined to be from 21.6 °C to 31.1 °C. Accordingly, in the LCT experiments the cooling wall and
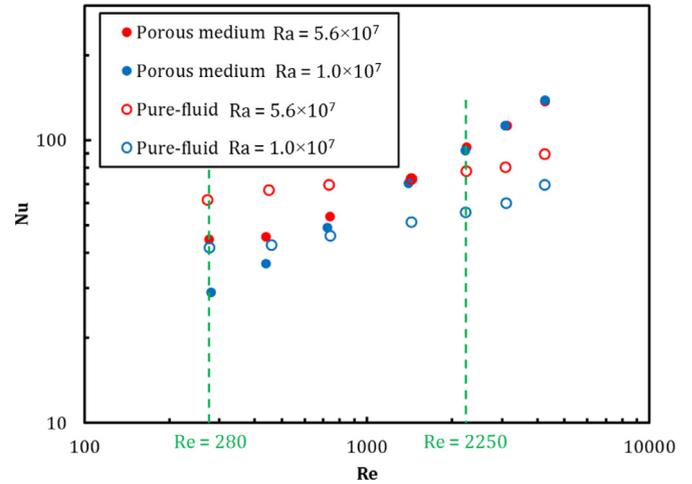
Fig. 2. Nu-Re data for the porous medium filled cavity compared to the pure-fluid cavity at two different Rayleigh numbers in configuration A.

the inflow temperatures were set to $T_{in} = T_c = 21.6$ °C, and the heating wall temperature was set to $T_h = 31.1$ °C which leads to a Rayleigh number of Ra $= 3.5 \times 10^7$. The color images of the thermochromic liquid crystals were finally converted to quantitative temperature fields based on a temperature-hue calibration procedure which is described in [24].

3. Results and discussions

3.1. Flow and heat transfer in the cavity with and without porous media

The Nusselt number was measured as a function of Reynolds number in the vented cavity with an inlet at the top of the heating wall and outlet at the bottom of the cooling wall (Configuration A, see Fig. 1b). The Nusselt numbers were measured both in the pure-fluid cavity without porous medium and in the same cavity filled with a porous medium consisting of a BCT packing of $d/H = 0.2$ spheres to identify the effect of the porous medium on the heat transfer. Fig. 2 shows the resulting Nu-Re data for two different Rayleigh numbers. It is observed that the heat transfer rate from the heating wall increases with Reynolds number in all cases. However, the slope of the Nu-Re curve is higher for the porous medium filled cavity. At low values of the Reynolds number, where natural convection dominates, the Nusselt number is higher for the pure-fluid cavity. This is consistent with what is reported for natural convection in side-heated cavities with and without porous media [25]. When increasing the Reynolds number, the Nusselt numbers for the porous medium filled cavity exceed those for the pure-fluid cavity. Fig. 3 shows that at low Reynolds number ($Re = 280$) in the porous medium filled cavity a portion of the cold inflow tends to move downward opposing the upward moving natural convection flow. However, in this case, the upward directed natural convection flow is sufficiently strong to prevent the cold inflow from reaching the hot wall. In this situation, hot fluid gets trapped in the region near the heating wall due to the presence of the spheres and the opposing inflow, resulting in a heat transfer rate lower than that for the pure-fluid cavity. However, as the Reynolds number increases, the forced convection gradually overcomes the natural convection such that a large portion of the cold inflow moves downward and comes in direct contact with the heating plate. This phenomenon causes a steep rise of Nusselt number with increasing Reynolds number. In contrast, in the pure-fluid cavity, the mechanism of heat removal and the flow pattern near the heating wall is qualitatively the same at
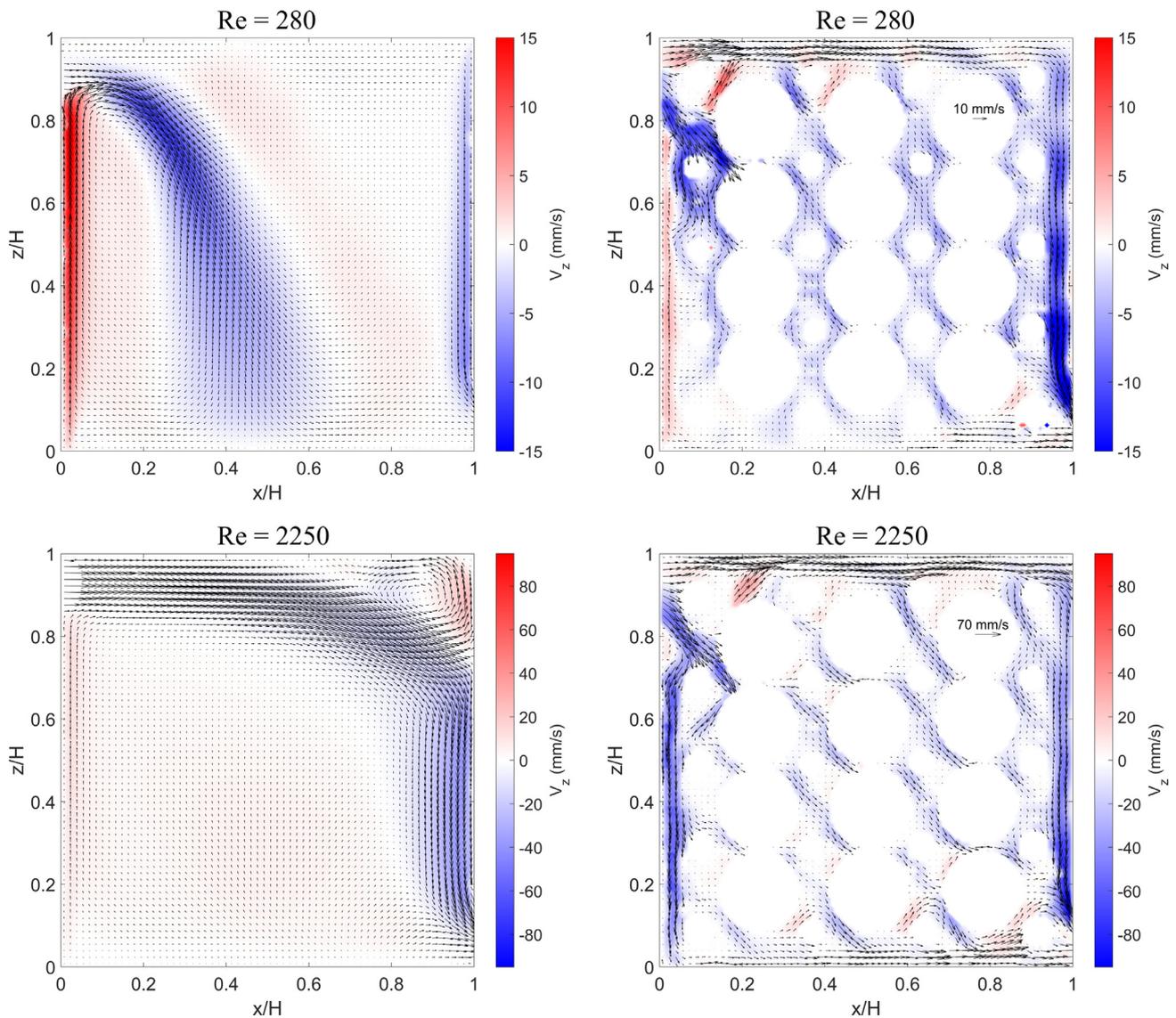
Fig. 3. Mean velocity fields at Ra = 5.6×10^7 for the pure-fluid cavity (left) and the porous medium filled cavity (right) at *Re* = 280 (top) and *Re* = 2250 (bottom) in configuration A. The color map represents the vertical velocity component v_z.

low and high Reynolds numbers. The forced convection flow favors heat removal by aiding the natural convection flow, but the cold fluid never comes into direct contact with the heating wall. As the Reynolds number increases, the inflow moves more straight through the cavity and then impinges on the cold wall. The flow and heat transfer in similar configurations without porous media are discussed in more detail in [2,9,10].

3.2. Effect of Rayleigh and Reynolds numbers on flow and heat transfer

Fig. 4 shows the Nusselt number as a function of Rayleigh number for six different Reynolds numbers including *Re* = =0 (corresponding to pure natural convection) for the cavity filled with the porous medium. Natural convection data for a side-heated closed cavity filled with the same porous medium [25] is also included for comparison. A good agreement between the slope of the two natural convection curves is observed. The shift in the values is due to the different geometries of the hot/cold walls (with and without inflow/outflow ports) and thus different length scales used to define the Rayleigh and Nusselt numbers. First, it is observed that the

mixed convection heat transfer is always higher than pure natural convection (*Re* = =0). This is due to introducing a cold fluid into the cavity which enhances the heat transfer from the heating plate to the fluid through a lowering of the bulk temperature. Second, it can be observed that at a constant Reynolds number *Re* > 0, the slope of the Nu-Ra curve is (nearly) zero at low Rayleigh numbers, and that this slope gradually increases with increasing Rayleigh number. This process also depends on the Reynolds number. The higher the Reynolds number, the later (in terms of Rayleigh number) the increase of the Nusselt number sets in and the smaller is the slope. In general, at higher Reynolds numbers and lower Rayleigh numbers (i.e. lower Ri), when forced convection is the dominant heat transfer regime, the Nusselt number becomes independent of the Rayleigh number and the scaling exponent α in Nu ~ Ra^α is zero. However, at lower Reynolds numbers and higher Rayleigh numbers (i.e. higher Ri), when natural convection is important, the value of the scaling exponent α increases. The highest scaling exponent is observed at the highest Rayleigh number and the lowest Reynolds number (i.e. the highest Ri) and is approximately 0.5.
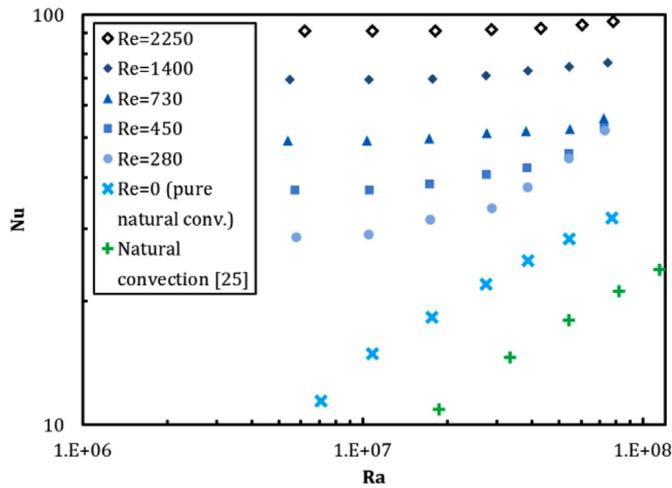
Fig. 4. Nu-Ra data for the porous medium filled cavity for different Reynolds numbers (configuration A). The crosses ($\times$) pertain to the pure natural convection data for the same porous medium filled vented cavity with no inflow. The pluses ($+$) pertain to data for natural convection in a closed cavity filled with the same porous medium [25].
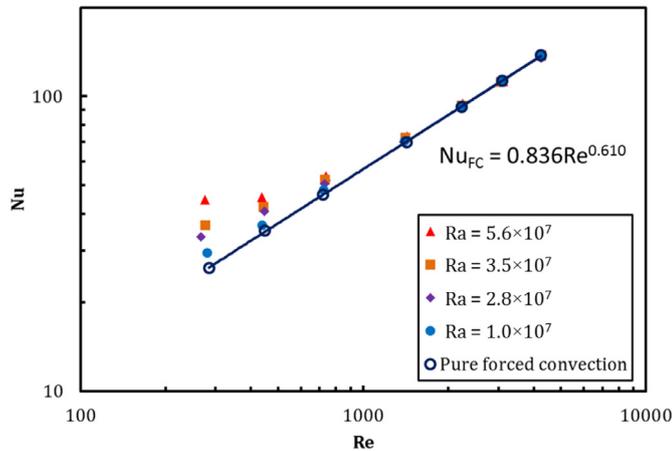
Fig. 5. Nu-Re data for the porous medium filled cavity for different Rayleigh numbers (configuration A). The solid line shows the power-law fit to the pure forced convection data, Eq. (6), for the same cavity.

Fig. 5 shows the Nusselt number as a function of Reynolds number at different Rayleigh numbers, along with the results for pure forced convection. The pure forced convection data points were obtained by rotating the cavity such that the heating plate is at the top and the cooling plate is at the bottom (see configuration C in Fig. 1b). The pure forced convection data points are fitted by the power-law

$$\mathrm{Nu_{FC}} = 0.836\,Re^{0.610}, \tag{6}$$

which is shown as a solid line in Fig. 5. It is observed that at sufficiently high Reynolds numbers, the heat transfer rates for different Rayleigh numbers converge to the forced convection curve. This indicates that natural convection is negligible in this range of high Reynolds numbers and that the flow and heat transfer are fully dominated by forced convection. For the highest Rayleigh number, the heat transfer data start to branch away from the forced convection curve when the Reynolds number decreases below approximately $Re = 1400$. This is an indication of the onset of natural convection effects. The Reynolds number where branching first occurs increases with increasing Rayleigh number. It is observed that at the highest Rayleigh number (i.e. Ra $= =5.6 \times 10^7$) and the lowest Reynolds numbers, the Nusselt number becomes almost indepen-

Table 1
The temperatures of the inflow, the cold wall, and the hot wall, and the bulk inlet velocities for the velocity and temperature fields shown in Figs. 8 and 9.

Ra	Re	Ri	$T_c = T_{in}$ (°C)	T_h (°C)	u_{in} (mm/s)
3.5×10^7	240	90.0	22.0	31.6	3.03
3.5×10^7	730	9.73	22.0	31.6	9.20
3.5×10^7	1400	2.65	22.0	31.6	17.6
3.5×10^7	2250	1.02	22.0	31.6	28.2

dent of Reynolds number such that the scaling exponent β in Nu $\sim Re^\beta$ approaches zero. This is an indication of the dominance of natural convection over forced convection. Fig. 6 shows the mean velocity fields at low Reynolds number ($Re = =280$) for three different Rayleigh numbers. It is seen that at this low Reynolds number, increasing the Rayleigh number substantially changes the flow structure in the vicinity of the heating wall so that the upward natural convection flow gradually overcomes the imposed downward forced convection flow. This leads to an enhanced strength of natural convection at a fixed forced flow and therefore the Nusselt number increases with increasing Rayleigh number. On the other hand, Fig. 7 confirms that at high Reynolds numbers, forced convection fully dominates the flow structure and natural convection flow is completely suppressed, such that increasing the Rayleigh number has no influence on the flow field and the heat transfer.

Fig. 8 shows the mean velocity fields at Ra $= 3.5 \times 10^7$ for four different Reynolds numbers. It shows that by increasing Reynolds number, the downward forced convection flow overcomes the upward natural convection flow in the region near the heating wall. The flow field results show that for $Re \gtrsim 1400$ the forced convection dominated regime is reached, such that a further increase of the Reynolds number (from 1400 to 2250) does not change the flow structure in the cavity. This is in agreement with the Nu-Re data in Fig. 5 which indicate that an asymptotic forced convection dominated regime is reached for $Re \gtrsim 1400$. Liquid Crystal Thermography (LCT) measurements were performed at the fixed Rayleigh number of Ra $= =3.5 \times 10^7$ based on the effective temperature range of the used liquid crystals. Fig. 9 shows the resulting mean temperature fields for the same four Reynolds numbers as in Fig. 8. The temperature measurement results show that at the lowest Reynolds number, due to the opposing behavior of the forced flow and the presence of the spheres, the hot fluid is trapped in a recirculation zone near the heating wall leading to the formation of a high-temperature isolated region in the vicinity of the heating wall. Since the downward forced flow is not strong enough to overcome the upward natural convection flow, the interaction between the cold inflow and the heating wall is minimal. This explains the low slope of the Nu-Re curve in this regime, see Fig. 5. As the Reynolds number increases and the downward forced convection flow overcomes natural convection, a larger portion of the inflow moves downward along the heating wall and subsequently along the bottom wall. As a result, the cold inflow interacts more directly with the heating wall and carries away the heat toward the outlet. For $Re \gtrsim 1400$, where forced convection dominates, it is observed that the cold inflow is in direct contact with the heating wall and the high-temperature region is driven away from the heating wall towards the bottom wall. This apparently leads to a higher sensitivity of the Nusselt number to variations in Reynolds number, and, as evidenced by the relatively large value of the scaling exponent in Eq. (6), the scaling exponent β in Nu $\sim Re^\beta$ becomes $\beta = 0.61$.

The boundary condition values corresponding to the velocity and temperature fields in Figs. 8 and 9 are given in Table 1.

(a) Ri = 18.9   (b) Ri = 52.9   (c) Ri = 105.8
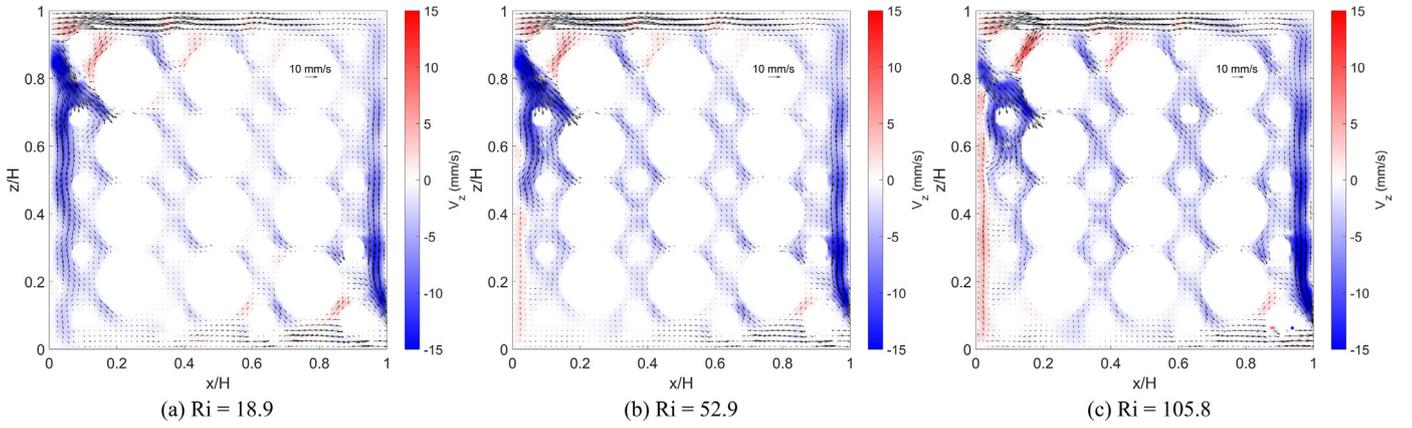
Fig. 6. Mean velocity fields at $Re = 280$ for (a) Ra = 1.0×10^7, (b) Ra = 2.8×10^7, and (c) Ra = 5.6×10^7 in configuration A.

(a) Ri = 0.29   (b) Ri = 0.82   (c) Ri = 1.65
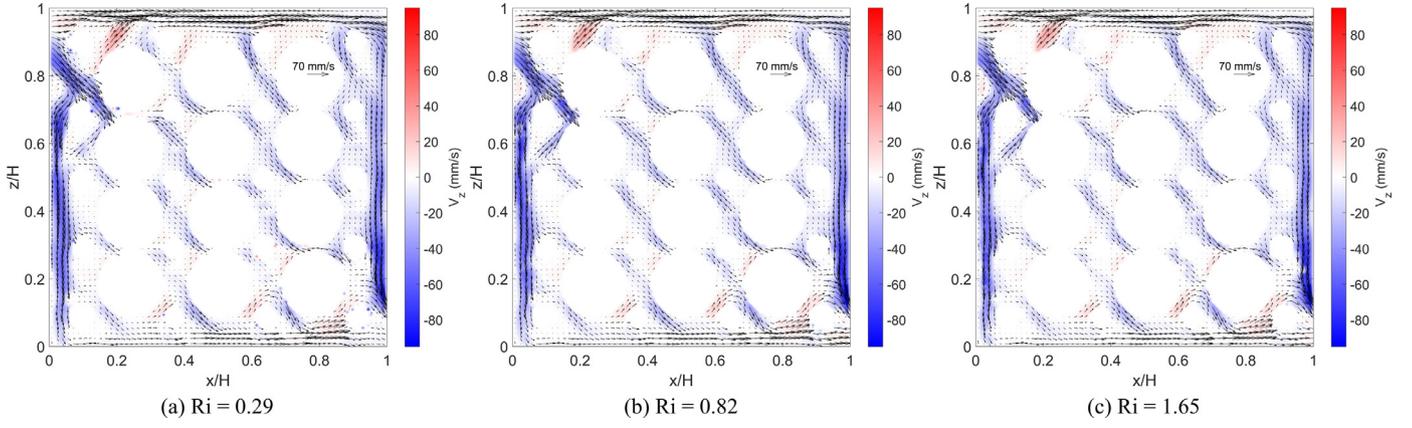
Fig. 7. Mean velocity fields at $Re = 2250$ for (a) Ra = 1.0×10^7, (b) Ra = 2.8×10^7 and (c) Ra = 5.6×10^7 in configuration A.

3.3. Effective scaling of Nusselt number

The results in Figs. 4 and 5 clearly imply that the Nusselt number is governed by the relative strength of natural and forced convection which can be represented by the Richardson number as discussed earlier in the introduction. Fig. 10 shows the ratio of the mixed convection heat transfer over the forced convection heat transfer (at the same Re) as a function of Richardson number for all measurements. The heat transfer data cover a wide range of Richardson numbers, i.e., $0.1 < Ri < 100$. It is observed that the data collapse onto a single curve which can represent the mixed convection heat transfer behavior in this configuration. Fig. 10 shows that for Ri $\lesssim 3$ the normalized Nusselt number is close to unity which indicates the dominance of forced convection over natural convection. This can be observed in the flow fields in Figs. 7, 8c, and d. The onset of natural convection effects corresponds to the point where the normalized heat transfer starts to deviate from unity at Ri ≈ 3. That is when natural convection flow emerges at the heating wall and by further increasing the Richardson number, it starts to take over the forced convection flow, see Figs. 6, 8a, and b. At Ri $\gtrsim 3$ the increasing strength of the natural convection results in an enhanced heat transfer with respect to the pure forced convection. A curve is fitted to the data points considering the constraints at the two extremes: (i) Nu being independent of Ra for Ri $\rightarrow 0$, and (ii) Nu being independent of Re for Ri $\rightarrow \infty$. The fitted curve is shown as a solid (green) line in Fig. 10 and is given by

$$\frac{Nu}{Nu_{FC}} = (1 + 0.0375 \, Ri)^{0.305}. \tag{7}$$

Substituting the power-law relation obtained for the forced convection heat transfer, Eq. (6), into Eq. (7) yields the following correlation for the Nusselt number as a function of Reynolds and Rayleigh number for low-conductivity spheres ($k_s/k_f \leq 1$)

$$Nu = 0.836 Re^{0.610}\left(1 + 0.00556\frac{Ra}{Re^2}\right)^{0.305}. \tag{8}$$

In this correlation, for Ri $\rightarrow 0$, the forced convection power-law function of Reynolds number, Eq. (6), is retrieved. Also, for Ri $\rightarrow \infty$, the Nusselt number scales with Ra$^{0.305}$ which is in agreement with classical natural convection scaling in cavities without porous medium [27]. As discussed in [24,25], natural convection scaling in porous media behaves very similar to the pure-fluid natural convection scaling at sufficiently high Rayleigh numbers. Both pure forced convection and pure natural convection asymptotes are shown in Fig. 10 as well.

Several theoretical studies of mixed convection along vertical flat plates have proposed correlations in the form of $Nu^n = Nu_{FC}{}^n + Nu_{NC}{}^n$ [28,29], where Nu_{FC} and Nu_{NC} are the forced convection and the natural convection asymptotes for Ri $\rightarrow 0$ and Ri $\rightarrow \infty$, respectively. Different values for n have been proposed: $n = 2$ [30], $n = 3$ [29,31], and $n = 4$ [28]. We found that for $n = 3$, the correlation agrees very well with our experimental data. The resulting correlation

$$\frac{Nu}{Nu_{FC}} = \sqrt[3]{1 + \left(\frac{Nu_{NC}}{Nu_{FC}}\right)^3} \tag{9}$$

is plotted in Fig. 10 as a dashed line.
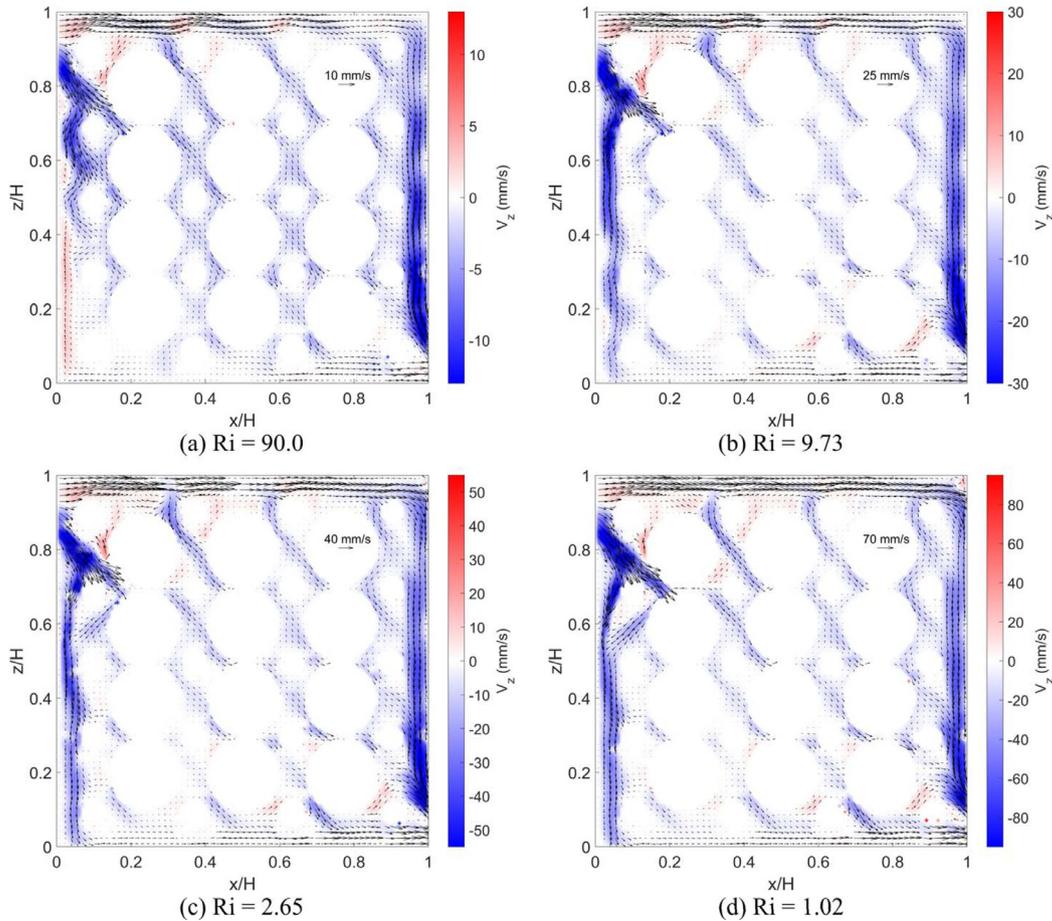
Fig. 8. Mean velocity fields at Ra = 3.5 × 10⁷ for (a) *Re* = 240, (b) *Re* = 730, (c) *Re* = 1400, (d) *Re* = 2250 in configuration A.

Another way of presenting the heat transfer data is to normalize the mixed convection heat transfer as follows

$$\text{Nu}_{\text{eff}}(Re,\ \text{Ra}) = \frac{\text{Nu}\ (\text{Ra},\ Re)}{\text{Nu}_{\text{NC}}(\text{Ra}) + \text{Nu}_{\text{FC}}(Re) - 1}. \quad (10)$$

Nu_{eff} is the effective Nusselt number and is used to quantify the strength of mixed convection heat transfer Nu (Ra, *Re*) with respect to the sum of the pure natural convection heat transfer at that specific Rayleigh number Nu_{NC} (Ra) and the pure forced convection heat transfer at that specific Reynolds number Nu_{FC} (*Re*). Since the conductive heat transfer is included in both Nu_{NC} and Nu_{FC}, 1 is subtracted from the sum to make sure that conduction is only considered once in the denominator. Fig. 11 shows the values of Nu_{eff} as a function of Richardson number for all heat transfer data points. It is observed that $\text{Nu}_{\text{eff}} < 1$ for the entire range of Richardson numbers considered in this study. For Ri < 10, the effective Nusselt number decreases with increasing Richardson number, which means that the enhancement of buoyancy-induced heat transfer is not as much as what it would be in the pure natural convection case. This is due to the fact that natural convection is mostly suppressed by the strong forced convection in this range of Ri numbers. In this regime, forced convection dominates and the heat transfer is determined by the Reynolds number since the heat transfer reduction caused by decreasing the Reynolds number is stronger than the heat transfer enhancement caused by increasing the Rayleigh number. The decrease of the effective Nusselt number continues until a minimum is reached in the intermediate range 10 < Ri < 40. Maximum competition between natural and forced convection occurs in this region which leads to the lowest effective Nusselt number. In this transitional regime, forced

and natural convection have comparable strength acting opposite each other, and therefore the effective heat transfer is insensitive to changes in Richardson number. For Ri > 40, the effective Nusselt number starts to increase with increasing Richardson number. In this regime, the Rayleigh number determines the heat transfer since the effect of increasing Rayleigh number is stronger than that of decreasing Reynolds number. The shape of the Nu_{eff} -Ri curve illustrates that in the studied configuration A (see Fig. 1), natural convection flow and forced convection flow work against each other as was readily seen in the flow fields in Figs. 6 and 8. In general, the shape of the Nu_{eff} -Ri curve enables us to identify three different flow and heat transfer regimes depending on Richardson number, namely a forced convection dominated regime (Ri < 10), a natural convection dominated regime (Ri > 40), and a transitional regime (10 < Ri < 40). These three regimes are shown in Fig. 11.

3.4. Effect of configuration on heat transfer

Although the majority of the experiments were conducted in configuration A, experiments were also performed in configuration B which has the inlet at the bottom of the heating wall and the outlet at the top of the cooling wall, see Fig. 1b. The Nu-*Re* data for the two configurations at two different Rayleigh numbers are compared in Fig. 12. The heat transfer behavior as a function of the Reynolds number and the Rayleigh number is qualitatively the same for both configurations, in the sense that there is 1) a general trend of increasing Nusselt number with increasing Rayleigh and Reynolds numbers, 2) Nusselt number is independent of Rayleigh number at high Reynolds numbers, and 3) Nusselt number only weakly depends on Reynolds number at low Reynolds numbers.
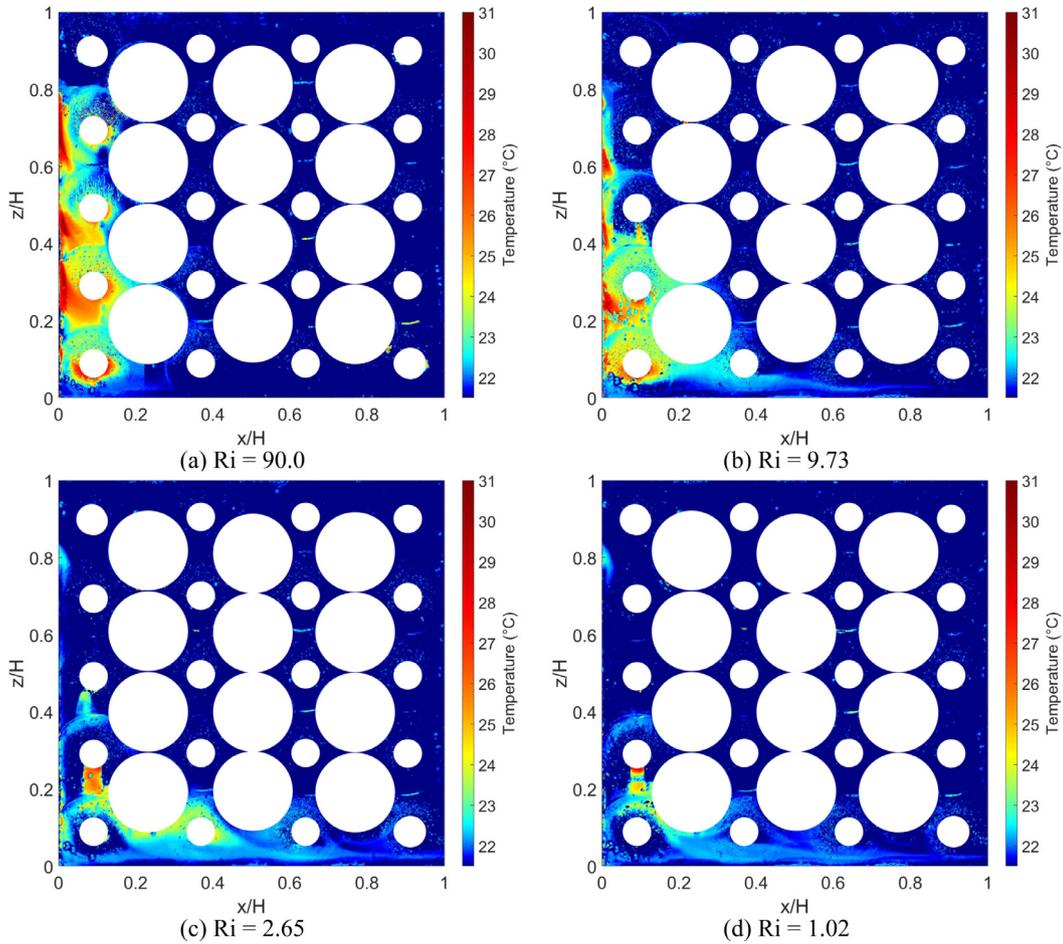
Fig. 9. Mean temperature fields at Ra = 3.5×10^7 for (a) Re = 240, (b) Re = 730, (c) Re = 1400, (d) Re = 2250 in configuration A.
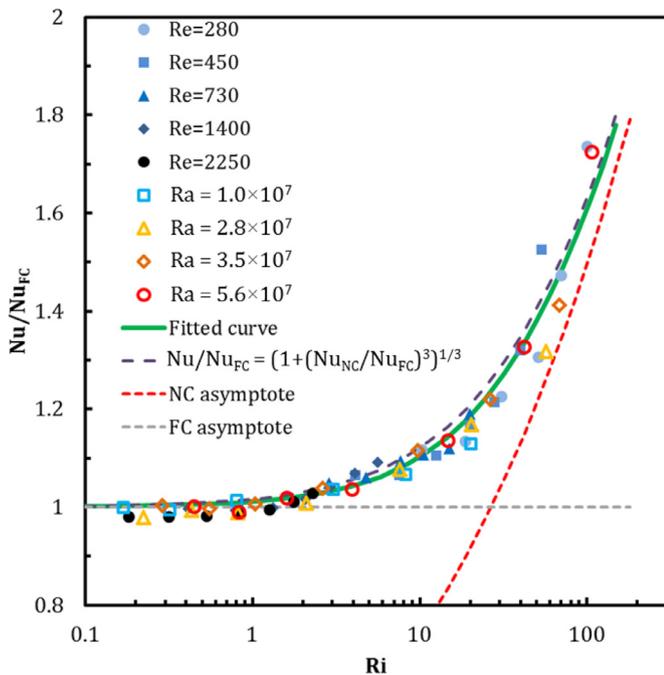
Fig. 10. Nusselt number, Nu, normalized with the pure forced convection Nusselt number, Nu$_{FC}$, as a function of Richardson number, Ri (configuration A). The (green) solid line shows the curve that was fitted to the data according to Eq. (7). The dashed line pertains to the correlation in Eq. (9).
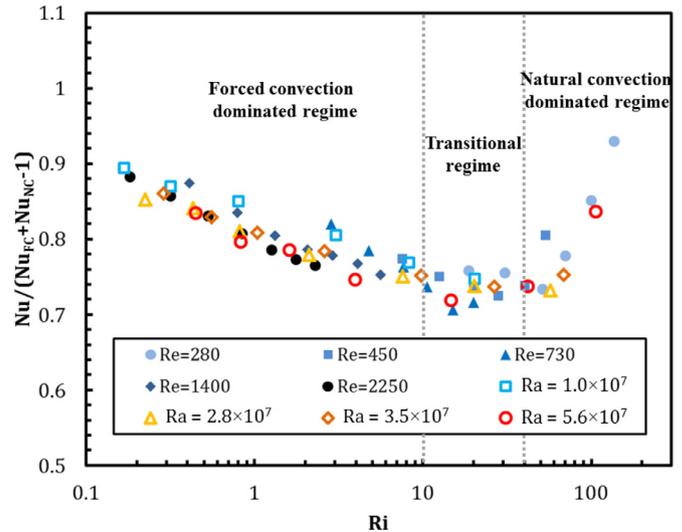
Fig. 11. Effective Nusselt number, Nu$_{eff}$ as a function of Richardson number, Ri in configuration A.

The graph shows that at sufficiently high Reynolds numbers (Re $\gtrsim$ 2000), the Nusselt numbers for both configurations converge to the forced convection curve, Eq. (6). As the Reynolds number decreases, the Nusselt number values for configuration B start to deviate from the forced convection curve and this deviation occurs at a higher Reynolds number than in configuration A. This
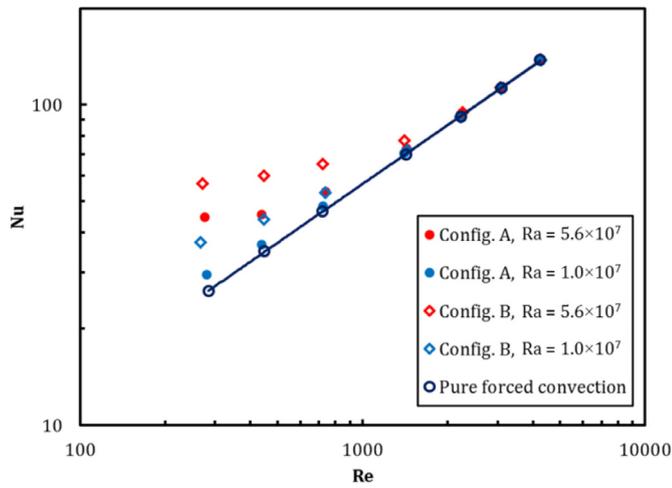
Fig. 12. Nu-*Re* data for configurations A and B at two different Rayleigh numbers.
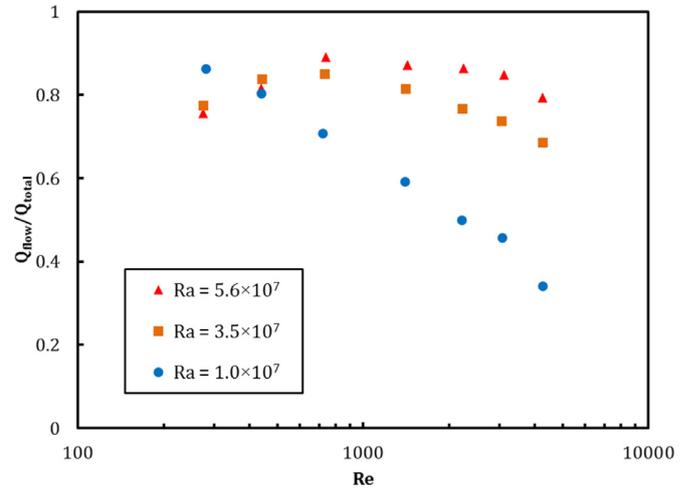
Fig. 13. The ratio Q_{flow}/Q_{total} as a function of Reynolds number for different Rayleigh numbers in configuration A.

Fig. 14. The ratio Q_{flow}/Q_{total} as a function of Rayleigh number for different Reynolds numbers in configuration A.

Fig. 15. The ratio Q_{flow}/Q_{total} as a function of Richardson number for all experiments (configuration A).

means that natural convection effects emerge earlier in configuration B and are clearly noticeable at Reynolds numbers as high as $Re = 1400$. At lower Reynolds numbers, where natural convection becomes more important, the configuration has a significant effect on the heat transfer, and the Nusselt numbers for configuration B are considerably higher than those for configuration A. This is most likely because in configuration B when natural convection is strong, a large portion of the cold incoming flow is entrained toward the heating wall by the upward buoyancy-induced natural convection flow. For $Re \gtrsim 2000$ natural convection flow is suppressed by the intense forced convection flow, thus the opposing and assisting behavior near the heating wall for Configurations A and B, respectively, have no influence on the flow structure and subsequently the heat transfer. In general, higher Nusselt numbers were measured for configuration B which implies that this configuration can extract more heat from the heating source and has a better heat removal performance compared to configuration A.

3.5. Heat removal splitting behavior

It is important to investigate how the heat from the heating wall is removed from the cavity. Part of the heat is transferred to the cooling wall which is kept at a low temperature equal to the inflow temperature. The remaining part is carried away by the flow and exits the cavity through the outlet. In this section, we study how the heat generated at the heating wall is distributed over these two heat removal pathways for configuration A. For this, we use the ratio Q_{flow}/Q_{total} as defined in Eq. (5). Figs. 13 and 14 show Q_{flow}/Q_{total} values as a function of Reynolds number for different Rayleigh numbers, and as a function of Rayleigh number for different Reynolds numbers, respectively. When shown as a function of Richardson number in Fig. 15, the results indicate a consistent behavior with a maximum at Ri ≈ 10. For Ri > 10 where natural convection flow is present at the heating wall, increasing the Richardson number (i.e. increasing Ra or decreasing *Re*) leads to a stronger upward natural convection flow overcoming the downward motion of the forced convection flow along the heating wall. This causes a larger portion of the forced inflow to move directly along the top and cold walls of the cavity leading to an increased heat transfer at the cold wall and, consequently, a reduced value of Q_{flow}/Q_{total}. This can be observed clearly in the mean velocity fields shown in Fig. 6. On the other hand, for Ri < 10 where forced convection dominates the flow structure, decreasing the Richardson number (i.e. increasing *Re* or decreasing Ra) leads to a decrease in Q_{flow}/Q_{total}. In the forced convection dom-

inated regime the inflow moves along both the hot/bottom walls and the top/cold walls. In this regime, as the Reynolds number increases, larger inertial forces cause the inflow to move more horizontally through the cavity and impinge on the cold wall which leads to a higher heat transfer at the cold wall and thus lower Q_{flow}/Q_{total} (see Fig. 13). Moreover, increasing the Rayleigh number in the forced convection dominated regime causes a higher heat transport along the hot/bottom walls and therefore an increased value of Q_{flow}/Q_{total} ratio (see Fig. 14). In general, the outflow is the main heat removal pathway at the intermediate range of Richardson numbers (Ri $\approx$ 10). However, as either natural convection or forced convection dominates, the cooling wall becomes a major heat removal pathway in this mixed convection configuration.
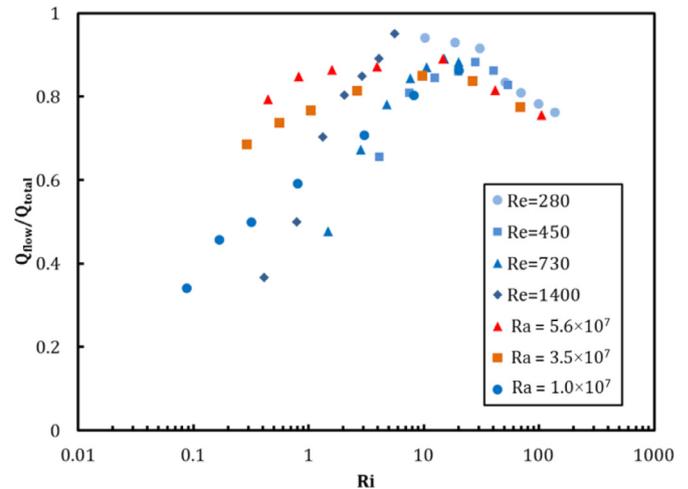
4. Conclusions

Mixed convection in a vented cavity (with an inlet at the top of the heating wall and an outlet at the bottom of the cooling wall) filled with a porous medium consisting of relatively large ($d/L = 0.20$) low-conductivity ($k_s/k_f \leq 1$) spheres was experimentally studied. Nusselt numbers, as well as velocity and temperature fields, were measured for a wide range of Reynolds and Rayleigh numbers resulting in a Richardson number variation between 0.1 to 100. For comparison, a pure-fluid cavity without porous medium and a second configuration with the inlet at the bottom of the heating wall and the outlet at the top of the cooling wall (configuration B) were also considered. It was found that at high Reynolds numbers, the Nusselt number is considerably higher for the cavity with porous medium as compared to the pure-fluid cavity due to a portion of the cold inflow directing toward the heating wall. For the cavity filled with spheres, a general trend of increasing Nusselt number with increasing Rayleigh and Reynolds numbers was observed. The Nusselt number normalized with the pure forced convection heat transfer depends only on the Richardson number which leads to the following correlation for the Nusselt number as a function of Reynolds and Rayleigh numbers (for $240 < Re <$ 4250, $6 \times 10^6 < Ra < 7 \times 10^7$ and $0.1 < Ri < 100$)

$$Nu = 0.836 Re^{0.610} \left(1 + 0.00556 \frac{Ra}{Re^2}\right)^{0.305}.$$

Based on the velocity fields and the behavior of the effective Nusselt number (which is defined as the Nusselt number normalized with the sum of pure natural and forced convection), three flow and heat transfer regimes can be identified depending on Richardson number: a forced convection dominated regime for Ri < 10; a transitional regime for $10 < $ Ri < 40; and a natural convection dominated regime for Ri > 40. In the forced convection dominated regime, natural convection flow is suppressed and both flow and heat transfer are very similar to those for the pure forced convection, and the Nusselt number scales with Reynolds number as Nu $\sim Re^{0.610}$, and is independent of the Rayleigh number. In the transitional regime, natural convection and forced convection flow are of comparable strength competing against each other which leads to a minimum effective Nusselt number and a maximum heat removal contribution by the outflow. In the natural convection dominated regime, the upward buoyancy-driven flow dominates and prevents the entrainment of the cold forced flow toward the heating wall. In that case, the Nusselt number is mainly determined by the Rayleigh number and only weakly depends on the Reynolds number. In configuration B, higher Nusselt numbers were measured in the natural convection dominated and transitional regimes which implies a better heat removal performance of this configuration.

References

[1] E. Papanicolaou, Y. Jaluria, Mixed convection from simulated electronic components at varying relative positions in a cavity, J. Heat Transfer 116 (2008) 960–970, doi:10.1115/1.2911472.

[2] E. Papanicolaou, Y. Jaluria, Mixed convection from an isolated heat source in a rectangular enclosure, Numer. Heat Transf. Part A Appl. 18 (1991) 427–461, doi:10.1080/10407789008944802.

[3] L. Koufi, Z. Younsi, Y. Cherif, H. Naji, Numerical investigation of turbulent mixed convection in an open cavity: effect of inlet and outlet openings, Int. J. Therm. Sci. 116 (2017) 103–117, doi:10.1016/j.ijthermalsci.2017.02.007.

[4] Q.-.H. Deng, J. Zhou, C. Mei, Y.-.M. Shen, Fluid, heat and contaminant transport structures of laminar double-diffusive mixed convection in a two-dimensional ventilated enclosure, Int. J. Heat Mass Transf. 47 (2004) 5257–5269 doi:10.1016/j.ijheatmasstransfer.2004.06.025.

[5] F.-.Y. Zhao, D. Liu, G.-.F. Tang, Multiple steady fluid flows in a slot-ventilated enclosure, Int. J. Heat Fluid Flow 29 (2008) 1295–1308 doi:10.1010.1016/j.ijheatfluidflow.2008.06.005.

[6] C.K. Cha, Y. Jaluria, Effect of thermal buoyancy on the recirculating flow in a solar pond for energy extraction and heat rejection, J. Sol. Energy Eng. 106 (1984) 428–437, doi:10.1115/1.3267622.

[7] C.K. Cha, Y. Jaluria, Recirculating mixed convection flow for energy extraction, Int. J. Heat Mass Transf. 27 (1984) 1801–1812, doi:10.1016/0017-9310(84)90162-5.

[8] A. Raji, M. Hasnaoui, Mixed convection heat transfer in a rectangular cavity ventilated and heated from the side, Numer. Heat Transf. Part A Appl. 33 (1998) 533–548, doi:10.1080/10407789808913953.

[9] S. Singh, M.A.R. Sharif, Mixed convective cooling of a rectangular cavity with inlet and exit openings on differentially heated side walls, Numer. Heat Transf. Part A Appl. 44 (2003) 233–253, doi:10.1080/716100509.

[10] A. Omri, S. Ben Nasrallah, Control volume finite element numerical simulation of mixed convection in an air-cooled cavity, Numer. Heat Transf. Part A Appl. 36 (1999) 615–637, doi:10.1080/104077899274606.

[11] D. Angirasa, Mixed convection in a vented enclosure with an isothermal vertical surface, Fluid Dyn. Res. 26 (2000) 219–233, doi:10.1016/S0169-5983(99)00024-6.

[12] J. Serrano-Arellano, J. Xamán, G. Álvarez, Optimum ventilation based on the ventilation effectiveness for temperature and CO2 distribution in ventilated cavities, Int. J. Heat Mass Transf. 62 (2013) 9–21, doi:10.1016/j.ijheatmasstransfer.2013.02.051.

[13] F.-.Y. Zhao, D. Liu, L. Tang, Y.-.L. Ding, G.-.F. Tang, Direct and inverse mixed convections in an enclosure with ventilation ports, Int. J. Heat Mass Transf 52 (2009) 4400–4412 10.1010.1016/j.ijheatmasstransfer.2009.03.017.

[14] E. Bilgen, A. Muftuoglu, Cooling strategy by mixed convection of a discrete heater at its optimum position in a square cavity with ventilation ports, Int. Commun. Heat Mass Transf. 35 (2008) 545–550, doi:10.1016/j.icheatmasstransfer.2008.01.001.

[15] S. Kenjereš, S.B. Gunarjo, K. Hanjalić, Contribution to elliptic relaxation modelling of turbulent natural and mixed convection, Int. J. Heat Fluid Flow 26 (2005) 569–586, doi:10.1016/j.ijheatfluidflow.2005.03.007.

[16] S. Murakami, S. Kato, T. Chikamoto, D. Laurence, D. Blay, New low-Reynolds-number k-ε model including damping effect due to buoyancy in a stratified flow field, Int. J. Heat Mass Transf. 39 (1996) 3483–3496, doi:10.1016/0017-9310(95)00356-8.

[17] S. Mahmud, I. Pop, Mixed convection in a square vented enclosure filled with a porous medium, Int. J. Heat Mass Transf. 49 (2006) 2190–2206, doi:10.1016/j.ijheatmasstransfer.2005.11.022.

[18] A.A. Bhuiyan, M.H. Banna, S.F. Barna, M.R. Amin, A.K.M. Sadrul Islam, Numerical modelling of thermal characteristics in a microstructure filled porous cavity with mixed convection, Int. J. Heat Mass Transf. 93 (2016) 464–476, doi:10.1016/j.ijheatmasstransfer.2015.10.004.

[19] N.S. Gibanov, M.A. Sheremet, M.A. Ismael, A.J. Chamkha, Mixed convection in a ventilated cavity filled with a triangular porous layer, Transp. Porous Media 120 (2017) 1–21, doi:10.1007/s11242-017-0888-y.

[20] N.O. Moraga, G.C. Sánchez, J.A. Riquelme, Unsteady mixed convection in a vented enclosure partially filled with two non-darcian porous layers, Numer. Heat Transf. Part A Appl 57 (2010) 473–495, doi:10.1080/10407781003659391.

[21] W.T. Cheng, C.N. Huang, S.W. Du, Three dimensional iron flow and heat transfer in the hearth of a blast furnace during tapping process, Chem. Eng. Sci. 60 (2005) 4485–4492, doi:10.1016/j.ces.2005.03.012.

[22] J.T. Hu, X.H. Ren, D. Liu, F.Y. Zhao, H.Q. Wang, Conjugate natural convection inside a vertical enclosure with solid obstacles of unique volume and multiple morphologies, Int. J. Heat Mass Transf. 95 (2016) 1096–1114, doi:10.1016/j.ijheatmasstransfer.2015.12.070.

[23] A. Ambaw, M.A. Delele, T. Defraeye, Q.T. Ho, L.U. Opara, B.M. Nicolaï, P. Verboven, The use of CFD to characterize and design post-harvest storage facilities: past, present and future, Comput. Electron. Agric. 93 (2013) 184–194, doi:10.1016/j.compag.2012.05.009.

[24] I. Ataei-Dadavi, M. Chakkingal, S. Kenjeres, C.R. Kleijn, M.J. Tummers, Flow and heat transfer measurements in natural convection in coarse-grained porous media, Int. J. Heat Mass Transf. 130 (2019) 575–584, doi:10.1016/j.ijheatmasstransfer.2018.10.118.

[25] I. Ataei-Dadavi, N. Rounaghi, M. Chakkingal, S. Kenjeres, C.R. Kleijn, M.J. Tummers, An experimental study of flow and heat transfer in a differentially side heated cavity filled with coarse porous media, Int. J. Heat Mass Transf. 143 (2019) 118591, doi:10.1016/j.ijheatmasstransfer.2019.118591.

[26] M. Chakkingal, S. Kenjereš, I. Ataei-Dadavi, M.J. Tummers, C.R. Kleijn, Numerical analysis of natural convection with conjugate heat transfer in coarse-grained porous media, Int. J. Heat Fluid Flow 77 (2019) 48–60, doi:10.1016/j.ijheatfluidflow.2019.03.008.

[27] G. Ahlers, S. Grossmann, D. Lohse, Heat transfer and large scale dynamics in turbulent Rayleigh-Bénard convection, Rev. Mod. Phys. 81 (2009) 503–537, doi:10.1103/revmodphys.81.503.

[28] A. Acrivos, On the combined effect of forced and free convection heat transfer in laminar boundary layer flows, Chem. Eng. Sci 21 (1966) 343–352, doi:10.1016/0009-2509(66)85027-3.

[29] S.W. Churchill, A comprehensive correlating equation for laminar, assisting, forced and free convection, AIChE J 23 (1977) 10–16, doi:10.1002/aic.690230103.

[30] J.C. Hsieh, T.S. Chen, B.F. Armaly, Nonsimilarity solutions for mixed convection from vertical surfaces in porous media: variable surface temperature or heat flux, Int. J. Heat Mass Transf. 36 (1993) 1485–1493, doi:10.1016/S0017-9310(05)80059-6.

[31] T.S. Chen, B.F. Armaly, N. Ramachandran, Correlations for laminar mixed convection flows on vertical, inclined, and horizontal flat plates, J. Heat Transfer 108 (1986) 835–840, doi:10.1115/1.3247020.